

RESEARCH ARTICLE | OCTOBER 23 2023

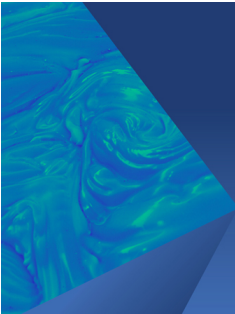
# Richtmyer–Meshkov instability of a single-mode heavy–light interface in cylindrical geometry

Jiaxuan Li (李佳轩) ; He Wang (王何) ; Zhigang Zhai (翟志刚)  ; Xisheng Luo (罗喜胜) 



*Physics of Fluids* 35, 106112 (2023)

<https://doi.org/10.1063/5.0167248>




## Physics of Fluids

Special Topic:

John Michael Dealy (1937-2024): Celebrating His Life  
Guest Editors: Alan Jeffrey Giacomini and Savvas G. Hatzikiriakos

[Submit Today!](#)



# Richtmyer–Meshkov instability of a single-mode heavy–light interface in cylindrical geometry

Cite as: Phys. Fluids **35**, 106112 (2023); doi: 10.1063/5.0167248

Submitted: 11 July 2023 · Accepted: 2 October 2023 ·

Published Online: 23 October 2023



View Online



Export Citation



CrossMark

Jiaxuan Li (李佳轩),<sup>1</sup> He Wang (王何),<sup>1</sup> Zhigang Zhai (翟志刚),<sup>1,a)</sup> and Xisheng Luo (罗喜胜)<sup>1,2</sup>

## AFFILIATIONS

<sup>1</sup>Advanced Propulsion Laboratory, Department of Modern Mechanics, University of Science and Technology of China, Hefei 230026, China

<sup>2</sup>State Key Laboratory of High Temperature Gas Dynamics, Institute of Mechanics, Chinese Academy of Sciences, Beijing 100190, China

<sup>a)</sup> Author to whom correspondence should be addressed: [sanjing@ustc.edu.cn](mailto:sanjing@ustc.edu.cn)

## ABSTRACT

Richtmyer–Meshkov (RM) instability of a single-mode SF<sub>6</sub>–air interface subjected to a convergent shock is investigated experimentally. The convergent shock tube is specially designed with an opening tail to weaken the Rayleigh–Taylor effect and eliminate the reflected waves' effect. The gas layer scheme is used to create a heavy gas environment at the upstream side of the interface. Before phase inversion is finished, the amplitude reduction is accelerated, but the Bell–Plesset (BP) effect in this process is found to be negligible. After phase inversion is completed, the linear growth rate is generally predicted due to small amplitude and the weak BP effect. In nonlinear regime, an existing nonlinear model is revised based on the Padé approximation to give a better prediction of amplitude growth. The spike amplitude grows almost linearly, whereas the bubble amplitude gradually saturates and even reduces. For a heavy–light interface in convergent geometry, although both the spike and bubble amplitude growths are promoted by the BP effect, the spike growth is more promoted than the bubble. The BP effect enhances generation of the second-order harmonic, which results in saturation and reduction of the bubble amplitude. The discrepancy in the BP effect between light-heavy and heavy-light interfaces is qualitatively demonstrated for the first time.

Published under an exclusive license by AIP Publishing. <https://doi.org/10.1063/5.0167248>

## I. INTRODUCTION

Richtmyer–Meshkov (RM) instability<sup>1,2</sup> develops at the interface of two impulsively accelerated fluids, each of different density. The initial perturbation amplitude grows continuously mainly due to pressure perturbation and baroclinic vorticity induction, and, finally, turbulent mixing may occur. This phenomenon was first theoretically investigated by Richtmyer<sup>1</sup> and later experimentally verified by Meshkov.<sup>2</sup> RM instability is closely related to the Rayleigh–Taylor (RT) instability,<sup>3,4</sup> which occurs when a light fluid accelerates a heavy fluid. However, RM instability occurs regardless of the relative position of the gases at the interface (heavy–light or light–heavy, i.e., the shock wave propagates from a heavy fluid to a light fluid or vice versa) and can be considered as an extension of the RT instability, where the constant acceleration of the interface is replaced by an impulsive acceleration. RM instability is an important phenomenon occurring in many applications at length and time scales spanning several orders of magnitude.<sup>5,6</sup> A substantial amount of effort has been invested in the RM instability studies in recent decades.

For a single-mode light-heavy interface, the perturbation amplitude initially grows and continues to grow after the shock impact.<sup>2,7–9</sup>

For a heavy-light interface, after the shock impact, the interface will experience a phase inversion, namely, the amplitude first reduces to zero and then grows in the opposite direction.<sup>10–13</sup> In the previous studies, the development of a single-mode perturbation induced by a shock wave in planar geometry has been greatly investigated. However, in real scenarios, RM instability often occurs in cylindrical or spherical geometry. In the convergent RM instability, the perturbation development will be affected by more mechanisms because both radial and angular directions are involved. Bell<sup>14</sup> and Plesset<sup>15</sup> first analyzed the early-time growth of the RT instability in cylindrical and spherical geometries and found that the perturbation growth rate varies with interface radius, referred to as the Bell–Plesset (BP) effect. In addition, for continuous radial flow behind the convergent shock, the interface is in a nonuniform pressure field as a whole, which inevitably introduces the RT effect.<sup>16–18</sup> Therefore, coupling of the BP effect, RT effect, and multiple impacts (shocks reflect back and forth between the interface and convergence center) greatly increases the complexity of the convergent RM instability.

Theoretically, Mikaelian considered a spherical system composed of multiple layers of concentric fluid shells and reported analytical

solutions for specific conditions.<sup>19–21</sup> The theory proposed by Mikaelian was further extended by Lombardini and Pullin<sup>22</sup> to predict the linear growth of three-dimensional perturbations induced by a convergent shock wave. Based on the perturbation expansion method, solutions to the perturbation growth in cylindrical geometry with accuracy, respectively, up to the third order<sup>23</sup> and fourth order<sup>24</sup> have been provided, and a nonlinear model based on the Padé approximation was proposed.<sup>25</sup> A weakly nonlinear model was derived by Wang *et al.*<sup>26</sup> (named the W-model hereinafter) through considering the growth of a small perturbation on a cylindrical interface between two incompressible fluids. This model, however, did not consider cylindrical motion of the balanced position of interface. Later, the W-model was further modified (named the mW-model hereinafter) to predict the development of the cylindrical interface subjected to arbitrary radial motion.<sup>27</sup> The stretching/compressing effect of the RM instability in convergent geometry was evaluated.<sup>28</sup> According to the nonlinear model for predicting the bubble evolution in planar geometry,<sup>29</sup> Zhao *et al.*<sup>30</sup> popularized this model to the RT instability induced by centripetal volumetric force in cylindrical geometry. In addition, theoretical modelings and numerical simulations on magnetohydrodynamic RM instability in convergent cylindrical geometry were also investigated.<sup>31–34</sup> Based on the Bell equation, a refined compressible model that considers the premixed width of the initial interface was proposed.<sup>35</sup> Also, a theoretical model for the convergent nonstandard RM instability considering baroclinic vorticity, geometric convergence, and nonuniform impact of a rippled shock was proposed.<sup>36</sup>

Experimentally, an annular coaxial vertical diaphragmless shock tube was designed, and the perturbation development in cylindrical geometry was studied.<sup>37</sup> By using the gas lens technique, a convergent shock was generated by refracting a planar shock at a light-heavy interface, and the development of a single-mode heavy-light perturbation was investigated.<sup>38</sup> Following this technique, experiments on heavy-light perturbation growths in cylindrical geometry have been conducted,<sup>39</sup> and the W-model<sup>26</sup> was modified based on the Padé approximation. The first measurements of single-mode perturbation amplitude in the convergent RM instability were performed by Ding *et al.*,<sup>17</sup> and the RT stabilization was found to reduce the growth rate. By taking the RT stabilization into account, a modified model based on the Bell equation was proposed to predict the perturbation growth before the arrival of the reflected shock from the convergence center (reshock for short hereinafter). The long-term effect of the RT stabilization even leads to a phase inversion on the single-mode light-heavy interface before reshock for appropriate initial conditions.<sup>40,41</sup> In these experimental studies, the BP effect, RT effect, and reshock are generally coupled together. To decouple them, a novel convergent shock tube was specially designed with an opening tail, i.e., the convergent shock leaves the test section without focusing,<sup>42</sup> and the nonlinear effect on the convergent RM instability of a light-heavy interface was highlighted.

Note that these experimental works in convergent geometry primarily focused on light-heavy interfaces. In inertial confinement fusion, the typical capsule consists of an outside ablator layer and an inside fuel layer, usually lighter than the ablator layer.<sup>5</sup> As a result, understanding the hydrodynamic instability caused by the interaction of a convergent shock wave with a heavy-light interface is vital. The development of a heavy-light interface subjected to a convergent shock is rarely investigated in experiments, probably because of the presence

of phase inversion which increases complexity of flow analysis, and difficulties encountered in creating a heavy gas environment. If the ambient gas at the upstream side of interface is not air, the first thing is to replace air by other heavy gas. However, it is difficult to ensure the uniformity of the heavy gas concentration, which greatly affects the stability of the convergent shock. Obviously, we can use air as the heavy gas, and helium, for example, as the light gas. Nevertheless, there are some limitations when using this gas combination. First, if helium is injected into the downstream side of the interface, the end of the test section must be sealed by using such as adhesive tape. Although the adhesive tape will be broken after the shock impact, the reflected shock will inevitably be generated and affect the evolving interface. Second, because the sound speed of helium is quite high, the shocked air-helium interface has a greater moving velocity. Due to the length limitation of the test section, the air-helium interface only evolves for about 200–300  $\mu\text{s}$  before it exits the test section. Considering the effect of the reflected shock, the evolving duration of the shocked interface will be more shortened. Third, it is difficult to clearly capture the transmitted shock wave in helium because of its weaker intensity. However, we need to determine the concentration of helium through comparing the velocities of the transmitted shock between experiment and one-dimensional theory. As a result, it would be better to use other heavier gas than air at the upstream side of the interface.

How the BP effect and nonlinearity behave in the heavy-light interface development induced by a convergent shock, and what are the differences of the RM instabilities between the heavy-light and light-heavy interfaces, remain unclear, which motivate the present work. In this work, a gas layer scheme is used to create a heavy gas environment. Except for the single-mode interface, an undisturbed interface is added at the upstream side of the single-mode one. Only air between these two interfaces is replaced by heavy gas. The soap-film technique is used to generate the undisturbed and single-mode interfaces. The experiments are conducted in the shock tube with an opening tail<sup>42</sup> to highlight the BP effect on the single-mode heavy-light interface. In the following part, the experimental methods are first provided, then the flow features and amplitude growth are qualitatively and quantitatively described. An existing nonlinear model is modified to better predict the amplitude growth. Finally, the difference in the BP effect on the developments of heavy-light and light-heavy interfaces is explained.

## II. EXPERIMENTAL METHODS

In this work, the development of a single-mode SF<sub>6</sub>-air interface subjected to a cylindrically convergent shock wave is investigated. To form an SF<sub>6</sub>-air interface, air in the upstream side of the interface must be replaced by SF<sub>6</sub>. However, we do not fill the whole driven section and test section with SF<sub>6</sub> because it will waste a lot of SF<sub>6</sub> in experiments, and it is difficult to determine and control the volume fraction of SF<sub>6</sub> in such a large space. Note that the non-uniformity of the gas concentration will result in an incident convergent shock with obvious perturbations. In this work, the gas layer scheme is used to form an SF<sub>6</sub>-air interface. As shown in Fig. 1(a), two soap-film interfaces, including a single-mode one and an undisturbed cylindrical one, are formed in the test section in advance. Then, the only thing is to replace air between these two interfaces by SF<sub>6</sub>. When a planar shock passes through the concave wall, a cylindrical shock is formed and converges along the oblique wall. As the cylindrical shock meets the undisturbed cylindrical interface, a cylindrical transmitted shock will

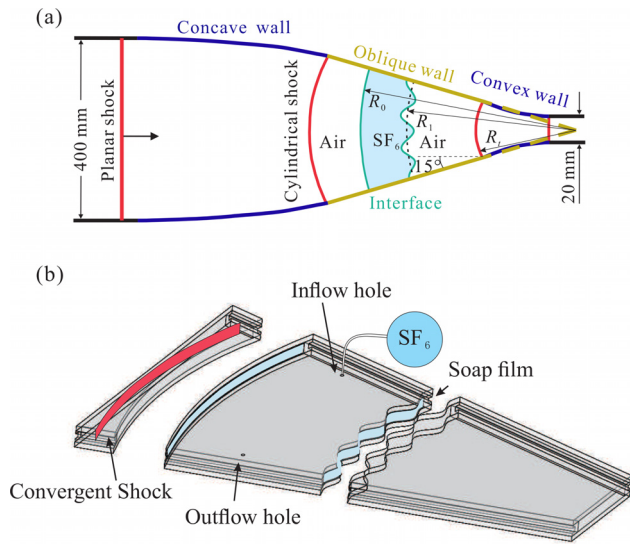


FIG. 1. Schematics of the convergent shock tube (a) and the interface formation device (b).

be generated in SF<sub>6</sub> and, subsequently, interacts with the single-mode SF<sub>6</sub>-air interface. The distance from the undisturbed interface to the single-mode interface is large enough (90 mm) to weaken the interface coupling effect and waves' effect.<sup>4,43</sup>

To generate a well-defined initial discontinuous interface, the soap-film technique<sup>44-46</sup> is used. Before the interface formation, three transparent devices, as shown in Fig. 1(b), are manufactured by combining two transparent acrylic plates (3.0 mm in thickness) with pedestals (7.0 mm in height). Two identical constraint strips (0.5 mm in width and 2.0 mm in height) are attached to the pre-carved grooves to constrain the soap-film. The ratio of the total height of the constraint strips protruding into the flow field (0.3 mm on each side) to the height of the whole flow field is smaller than 10%, and, thus, the constraint strips have negligible effects on the shocked flow.<sup>47</sup> To generate the soap-film interface, the constraint strips are wetted by the soap solution (78% pure water, 2% sodium oleate, and 20% glycerin by mass) in advance, then a rectangular brush with the soap solution attached is pulled carefully along the constraint strips, and, finally, the soap-film interface is generated. Afterward, SF<sub>6</sub> is injected into the space between these two interfaces through the inflow hole, and air is evacuated through the outflow hole. An oxygen concentration detector is placed at the outflow hole to monitor the concentration of SF<sub>6</sub>. Once the concentration of air is smaller than 0.5%, the inflation is stopped. Subsequently, the devices are joined together and gently inserted into the test section.

The single-mode interface studied in this work can be expressed as  $r(\theta) = R_1 + a_0 \cos(m\theta)$ , where  $R_1 = 235$  mm is the mean radius of the initial interface,  $a_0$  is the initial amplitude, and  $m$  is the azimuthal mode number. The variation of interface radial position can reflect the convergent effect, and the perturbation amplitude represents the degree of perturbation development in RM instability. Five cases labeled as  $m - a_0$ , as shown in Table I, are studied. For the first three cases (group I), the mode number is fixed to evaluate the effect of initial amplitude on flow features. For the last three cases (group II), we

TABLE I. Physical parameters for all cases.  $m$  is the azimuthal mode number of the perturbation,  $a_0$  is the initial perturbation amplitude at the boundary slice,  $a_v$  is the average perturbation amplitude,  $\lambda$  is the wavelength, and  $k$  is the perturbation wave-number.  $M_s$  is the Mach number of the incident shock.  $\psi(\text{SF}_6)$  is the SF<sub>6</sub> volume fraction within the gas layer, and  $A^+$  is the post-shock Atwood number.  $\Delta V$  is the experimental interface velocity jump by shock impact, and  $\Delta V^t$  is the theoretical value. The units for velocity, length, and time are  $\text{m s}^{-1}$ , mm, and  $\mu\text{s}$ , respectively.

Case	$m$	$a_0$	$a_v$	$\lambda$	$ka_v$	$M_s$	$\psi(\text{SF}_6)$	$A^+$	$\Delta V$	$\Delta V^t$
48-3.0	48	3.0	2.580	30.761	0.527	1.35	0.82	0.65	109.7	110.1
48-2.0	48	2.0	1.725	30.761	0.352	1.36	0.79	0.64	117.7	114.3
48-1.5	48	1.5	1.295	30.761	0.264	1.36	0.83	0.65	111.7	111.8
36-2.0	36	2.0	1.834	41.015	0.269	1.35	0.83	0.65	109.6	108.7
24-3.0	24	3.0	2.882	61.523	0.294	1.35	0.80	0.64	109.6	111.0

fix  $ma_0$  to evaluate the effect of mode number on flow features. The physical parameters for each case are shown in Table I. The boundary-layer effect was evaluated in the previous work<sup>48</sup> and found to be negligible. Three-dimensionality of the soap-film interface in cylindrical geometry can be expressed as follows:<sup>40</sup>

$$r(z, \theta) = R_1 \cosh(z/R_1) + a(z) \sin(m\theta - \pi/2),$$

where  $a(z)$  is the perturbation amplitude at the height  $z$  that can be solved numerically.<sup>40</sup> The integral average amplitude of the interface with minimum-surface feature ( $a_v$ ) is expressed as

$$a_v = \frac{\int_{-h}^h a(z) dz}{2h},$$

where  $h$  is the half height of the test section. The value of  $a_v$  for each case is provided in Table I. Three-dimensionality is more prominent for an interface with a large initial amplitude and short wavelength.

Experiments are conducted in a convergent shock tube with a smooth concave-oblique-convex wall designed to modify the shock shape,<sup>42</sup> as shown in Fig. 1(a). The present design enables a strong convergent shock near the convergence center to exit the convergent section without shock focusing and reflecting. Thus, the RT effect and reshock are eliminated. The post-shock flow field is recorded by high-speed schlieren photography. The frame rate of the high-speed video camera (FASTCAM SA-Z, Photron Limited) is set to be 67 200 frames per second, and the exposure time is 1.25  $\mu\text{s}$ . Due to the different sizes of observation domains required, the spatial resolution for different cases is within  $0.297 \pm 0.001$  mm pixel<sup>-1</sup>. The Mach number of the incident cylindrical shock wave when it reaches the single-mode SF<sub>6</sub>-air interface is  $1.35 \pm 0.01$ . The ambient pressure and temperature are  $101.3 \pm 0.1$  kPa and  $297.90 \pm 2.55$  K, respectively.

### III. RESULTS AND DISCUSSION

#### A. Background flows

Experimental schlieren images of the incident convergent shock (IS) interacting with the undisturbed cylindrical SF<sub>6</sub>-air interface are shown in Fig. 2(a). The time origin, i.e.,  $t = 0$   $\mu\text{s}$ , is defined as the moment when IS meets the initial interface (II). Initially, IS has a perfectly cylindrical shape ( $-82$   $\mu\text{s}$ ), and no obvious disturbance waves are observed behind it. These indicate that the gas layer scheme that



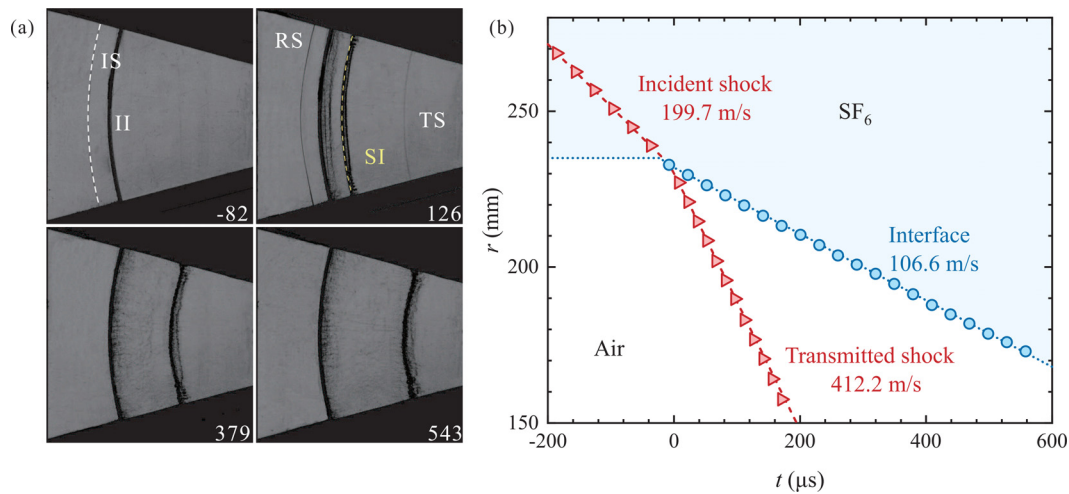


**FIG. 2.** (a) Experimental schlieren images of an undisturbed cylindrical  $\text{SF}_6$ -air interface induced by an IS. Numbers denote the time in  $\mu\text{s}$ . (b) The time-variation of displacements of shock waves and interface. IS, incident convergent shock; TS, transmitted shock; RS, reflected shock; II, initial interface; SI, shocked interface.

creates a heavy gas environment at the upstream side of the interface does not affect the quality of IS. After IS interacts with II, an upstream-propagating reflected rarefaction waves that are not observed in schlieren images due to their weak intensity and a downstream-moving transmitted shock (TS) are generated. An upstream-propagating reflected shock (RS) is also observed due to the reflection of IS from the filaments used to restrict the soap-film interface.<sup>49</sup> TS and RS also remain cylindrical shapes (126  $\mu\text{s}$ ). The shocked interface (SI) moves downstream also with a cylindrical shape. As late stages (543  $\mu\text{s}$ ), the interface profile becomes thicker due to the diffusion of soap droplets. Note that the rightmost dark line is the shocked interface, whereas the leftmost dark line represents the position of the filaments.

Figure 2(b) gives the time-variation of displacements of shock waves and SI. Their moving velocities are also provided by linearly fitting the data extracted from the central parts of their profiles. It is found that the shock waves and interface move almost linearly, and their velocities agree well with the predictions from one-dimensional gas dynamics. The constant velocity of SI indicates that the RT effect is negligible. Note that although the test section is designed with an opening end, there are waves emerging from the exit corners and reflecting to interact with the evolving interface. In the current work, the effective experimental time has ended before these reflected waves arrival.

## B. Perturbed interface morphologies and flow features

Experimental schlieren images of the single-mode  $\text{SF}_6$ -air interfaces accelerated by IS for different cases are shown in Fig. 3. The time origin is defined as the moment when IS arrives at the mean position of II. Taking case 48-3 as an example, after IS passes through II, a perturbed TS propagates downstream (56  $\mu\text{s}$ ). Note that the reflected shock (RS) from the filaments does not affect the interface development significantly since only the downstream interface is concerned.<sup>49</sup> The amplitude of SI first decreases after the shock impact and then reaches almost zero (101  $\mu\text{s}$ ). Afterward, the original peaks (troughs) become troughs (peaks), which is known as phase inversion. After

phase inversion, the amplitude of SI starts to develop in the opposite direction and increases gradually. Note that several shadow structures, marked by white dashed lines, follow the bubble front (190  $\mu\text{s}$ ). This phenomenon was also observed in the previous work,<sup>50</sup> in which the RM instability of a three-dimensional  $\text{SF}_6$ -air interface with a minimum-surface feature induced by a planar shock was investigated. The formation of these structures is possibly ascribed to the difference in pressure perturbation at different planes due to the minimum-surface feature of the interface. The soap droplets may also account for the formation of these structures. At late stages, spikes become longer and more tapered than bubbles, and the interface asymmetry becomes obvious (517  $\mu\text{s}$ ). For different cases, the interface morphologies are similar.

## C. Phase inversion and linear growth stages

Phase inversion is the specific phenomenon that occurs in the shocked heavy-light perturbation. The amplitude growth before and shortly after phase inversion is given in Fig. 4, in which the amplitude before phase inversion is defined as negative. Here, the amplitude is normalized as  $\alpha = am/R_0$ , and the time is normalized as  $\tau = v_w(t - t^*)m/R_0$ , with  $t^*$  being the time when phase inversion is completed and  $v_w$  being the linear growth rate, which will be discussed below. The amplitude is measured based on the central part of the interface profile, and error bars result from the thickness of the interface profile. The error bars seem significant because the amplitude scale is limited. Before phase inversion is finished, the amplitude reduction is accelerated as time proceeds. For the RM instability, actually, there is a startup process before the perturbation amplitude grows linearly. During the startup process, the amplitude growth is accelerated for a light-heavy interface,<sup>51</sup> whereas the amplitude reduction is accelerated for a heavy-light interface.<sup>52</sup> Yang *et al.*<sup>52</sup> proposed a linear model (the YZ-model) in planar geometry by constructing the velocity perturbations and pressure perturbations in different regions of the flow field. The YZ-model can predict the acceleration process of perturbation growth rate from zero to the linear one. Therefore, it is

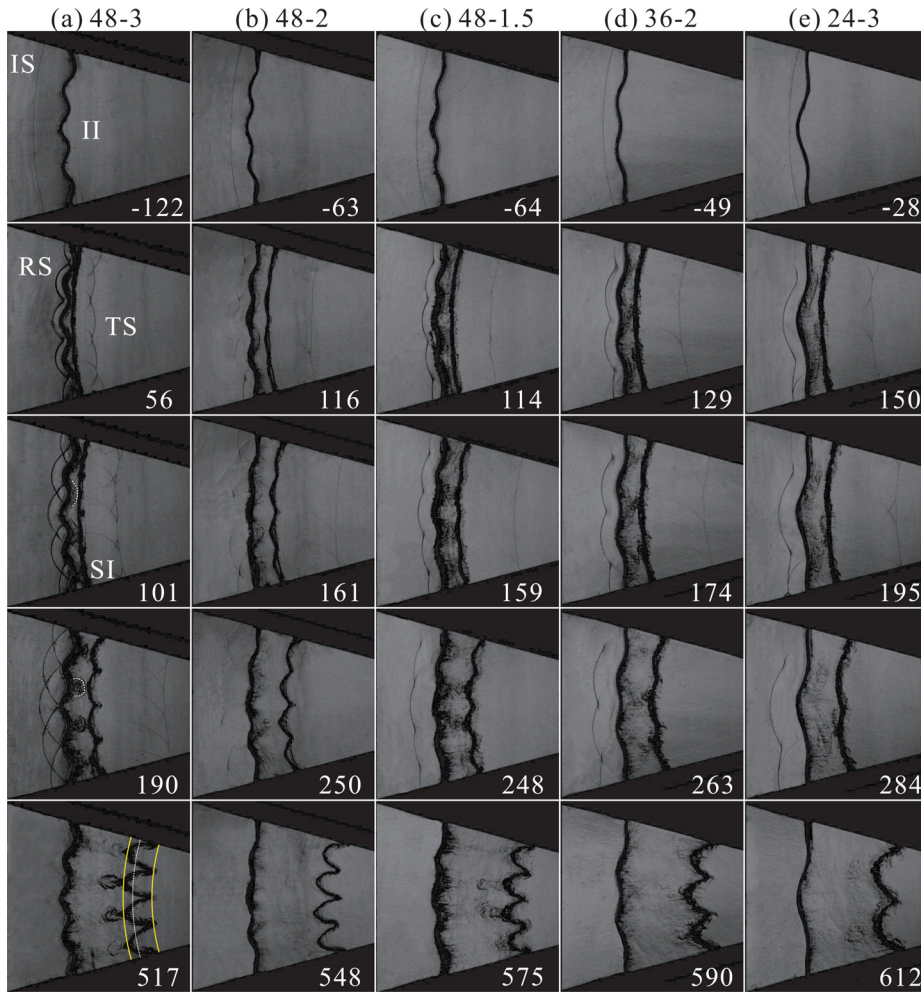


FIG. 3. Developments of single-mode SF<sub>6</sub>-air interfaces accelerated by IS for different cases. Symbols have the same meaning as those in Fig. 2.

08 April 2024 03:41:16

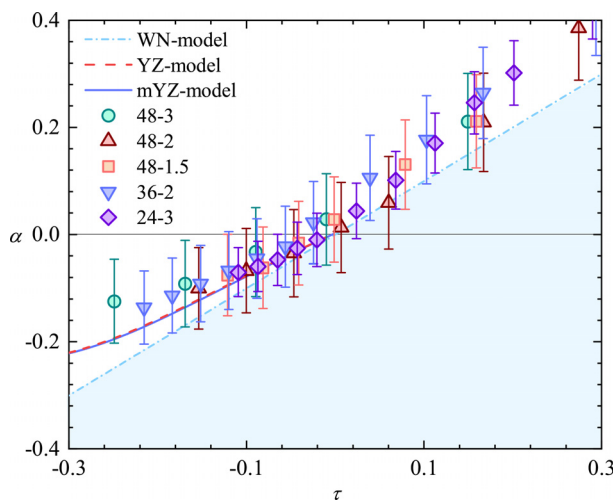


FIG. 4. Amplitude growths before and shortly after phase inversion.

possible to predict the startup process for the RM instability in planar geometry. As shown in Fig. 4, the YZ model generally predicts the acceleration process before phase inversion.

In convergent geometry, the BP effect always promotes amplitude growth, and, therefore, it prevents the interface from phase inversion. The stretching/compressing effect, a prominent part of the BP effect, is in proportion to the real-time amplitude of the interface.<sup>28</sup> As the amplitude decreases, the BP effect gradually weakens. Thus, the reduction rate of the amplitude before phase inversion increases. In other words, the BP effect also contributes to the acceleration of amplitude reduction.<sup>53</sup> To evaluate the BP effect, the YZ-model is extended to cylindrical geometry in this work. By considering the BP effect and by integrating the Bell equation,<sup>14</sup> the modified YZ model (the mYZ-model) can be expressed as

$$a_{mYZ} = a_0 + R_0^2 \int_{t_0^+}^t \frac{\dot{a}_{YZ}(t)}{R^2(t)} dt, \quad (1)$$

where  $\dot{a}_{YZ}(t)$  is the growth rate obtained by the YZ-model and  $t_0^+$  is the time just after shock passage. As shown in Fig. 4, the predictions

**TABLE II.** Comparison of the theoretical ( $v_w$ ) and experimental ( $v_e$ ) growth rates for all cases shortly after the phase inversion.  $v_w/\Delta V$  is the ratio of theoretical growth rate to interface jump velocity.

Case	48-3	48-2	48-1.5	36-2	24-3
$v_w$	-26.21	-17.60	-13.17	-13.96	-14.59
$v_e$	$-30.06 \pm 4.27$	$-22.96 \pm 2.46$	$-16.38 \pm 1.66$	$-18.28 \pm 1.11$	$-19.22 \pm 1.88$
$v_w/\Delta V$	-0.286	-0.188	-0.144	-0.154	-0.158

by the mYZ-model and YZ-model coincide, which indicates that the BP effect is negligible. Actually, the interface radius only reduces  $\sim 10$  mm before phase inversion, and, thus, the BP effect is negligible.

After phase inversion, the heavy-light perturbation amplitude generally starts to grow linearly in planar geometry.<sup>54</sup> In convergent geometry, however, the BP effect always exists and promotes amplitude growth. In the previous experiments conducted in the convergent shock tube with an opening tail,<sup>42</sup> the theory fails to predict the initial growth rate because the BP effect is stronger due to rapid change of interface radius. In this work, shortly after phase inversion, the interface amplitude is very limited. The additional amplitude growth rate induced by the BP effect is relatively weak compared with the growth rate imparted by the incident shock. To predict the linear growth rate of a heavy-light perturbation, the irrotational model proposed by Wouchuk and Nishihara<sup>55</sup> (named the WN model) is used, which can be expressed as

$$v_w = \frac{m}{R_0} a_v \left[ \frac{1+A^+}{2} (1 + V_t/V_i)(V_1 - \Delta V) + \frac{1-A^+}{2} (1 - V_t/V_i)\Delta V \right], \quad (2)$$

where  $V_i$ ,  $V_t$ ,  $V_r$ , and  $V_1$  are the velocities of the incident shock, transmitted shock, reflected rarefaction front, and the flow behind the incident shock, respectively. Comparison of the theoretical predictions and experimental measurements of the linear growth rates is provided in Table II. The WN model slightly underestimates the linear growth rates compared to the experimental values, probably because the BP effect induces an additional growth rate in experiments.

#### D. Nonlinear growth rate

The amplitude growths after phase inversion for groups I and II are presented in Figs. 5(a) and 5(b). The normalization method is the same as that in Fig. 4. The observed amplitude growths in group II collapse, which means the amplitude growth is insensitive to mode number under the conditions studied. However, the amplitude growths in group I deviate from each other as time proceeds. This deviation is probably ascribed to the significant difference in  $v_w/\Delta V$ , as shown in Table II, because the normalization method does not consider the interface convergence effect. At late stages, the amplitude growth rates begin to decrease due to increasing nonlinearity, and the amplitude even tends to saturate.

For the evolution of a heavy-light perturbation induced by a planar shock, a weakly nonlinear model proposed by Zhang and Guo<sup>56</sup> (named the ZG model) can be used to predict the amplitude growth rate. The ZG model can be expressed as

$$v_{ZG} = \frac{v_w}{1 + \phi k v_w t}, \quad (3)$$

where

$$\phi = \frac{3}{4} \frac{(1+A)(3+A)}{3+A+\sqrt{2}(1+A)^{1/2}} \times \frac{4(3+A) + \sqrt{2}(9+A)(1+A)^{1/2}}{(3+A)^2 + 2\sqrt{2}(3-A)(1+A)^{1/2}}. \quad (4)$$

The ZG model underestimates amplitude growth in convergent geometry, as shown in Fig. 5, mainly because the BP effect promotes

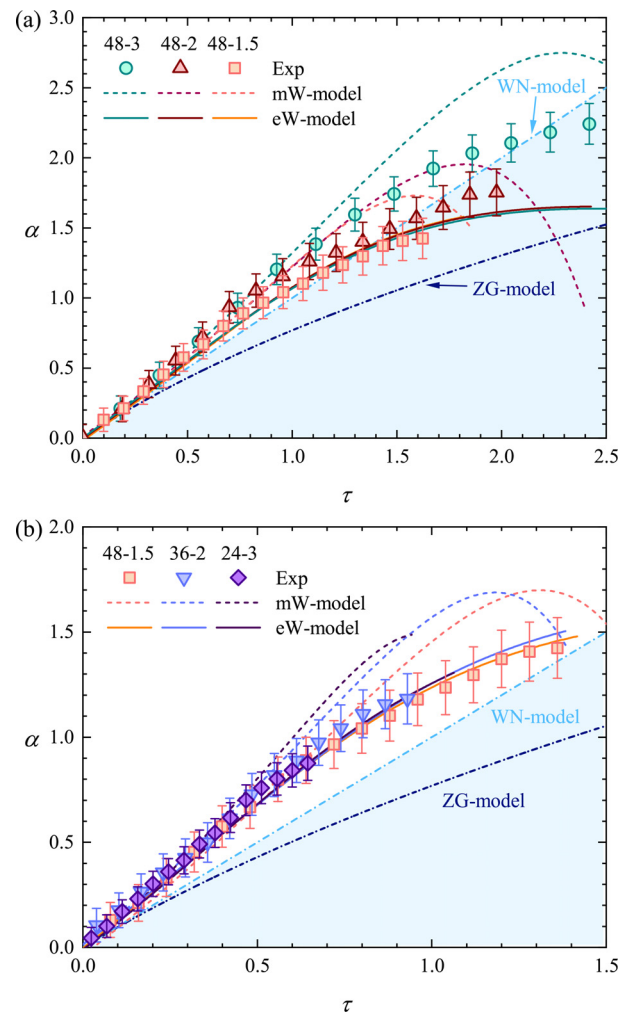


**FIG. 5.** Nonlinear evolutions of amplitude growth in group I (a) and group II (b).



amplitude growth (the interface radius moves more than 60 mm after phase inversion, and the BP effect is significant). Similar to the light-heavy interface,<sup>42</sup> the BP effect also inhibits nonlinearity and extends the linear regime in this work.

In convergent geometry, a weakly nonlinear model (the mW-model) was proposed by Wang *et al.*<sup>27</sup> to estimate amplitude growth of a cylindrical interface subjected to arbitrary radial motion, and an analytical solution up to the third order was given under a constant background flow. The expressions of the mW-model are provided in Appendix. Note that the positive Atwood number is defined for the heavy-light interface in the mW-model, which is different from the definition in the ZG model. The predictions from the mW-model for different cases are also provided in Fig. 5. Relative to the ZG model, the mW-model provides a better prediction to amplitude growth at early stages ( $\tau < 1.0$ ). Note that the BP effect promotes amplitude development, resulting in a larger linear growth rate than the prediction from the WN model. From intermediate stages, the mW-model overestimates the experimental results and even gives an incorrect prediction at late stages. Note that the mW-model contains higher order of  $\dot{a}_0$ . In our experiments,  $\dot{a}_0/\Delta V$  is much larger than the value given in the original paper of the mW-model, which probably causes the overestimation of the high-order components.

To extend the mW-model applicability, the Padé approximation is used. Because the mW-model is complicated and the Padé approximation is difficult to be executed directly, the mW-model is expanded into the Mclaurin series of time  $t$  first,

$$a_s = \sum_{i=0} \sigma_i t^i, \tag{5}$$

$$a_b = \sum_{i=0} \delta_i t^i, \tag{6}$$

where  $a_s$  and  $a_b$  are amplitudes of spike and bubble, respectively, and  $\sigma_0 = a_0$ ,  $\delta_0 = -a_0$ ,  $\sigma_1 = \dot{a}_0$ ,  $\delta_1 = -\dot{a}_0$ ,

$$\begin{aligned} \sigma_2 = & \frac{a_0^2 \dot{a}_0 (6 - 9Am + 2m^2) R_0 \Delta V + a_0^3 (A - 3m) m \Delta V^2}{4R_0^4} \\ & - \frac{a_0 \dot{a}_0 [\dot{a}_0 (-27 + 5m^2 + 3Am + 3A^2 m^2) + 12\Delta V]}{24R_0^2} \\ & - \frac{\dot{a}_0 (\dot{a}_0 + 2A\dot{a}_0 m - 4\Delta V) R_0 - 4a_0 \dot{a}_0 Am \Delta V}{4R_0^2}, \\ \delta_2 = & - \frac{a_0^2 \dot{a}_0 (6 - 9Am + 2m^2) R_0 \Delta V - a_0^3 (A - 3m) m \Delta V^2}{4R_0^4} \\ & + \frac{a_0 \dot{a}_0 [\dot{a}_0 (-27 + 5m^2 + 3Am + 3A^2 m^2) - 12\Delta V]}{24R_0^2} \\ & - \frac{\dot{a}_0 (\dot{a}_0 + 2A\dot{a}_0 m + 4\Delta V) R_0 - 4a_0 \dot{a}_0 Am \Delta V}{4R_0^2}. \end{aligned}$$

Because  $\sigma_1$  and  $\delta_1$  are irrelevant to time  $t$ , by taking the Padé approximation to the Mclaurin series, the extended model (named the eW-model) can be expressed as

$$a_s = \frac{\frac{\sigma_1 (\sigma_1^2 - 2\sigma_0 \sigma_2)}{\sigma_1^2 - \sigma_0 \sigma_2} t + \sigma_0}{\frac{\sigma_2}{\sigma_1^2 - \sigma_0 \sigma_2} t^2 - \frac{\sigma_1 \sigma_2}{\sigma_1^2 - \sigma_0 \sigma_2} t + 1}, \tag{7}$$

$$a_b = \frac{\frac{\delta_1 (\delta_1^2 - 2\delta_0 \delta_2)}{\delta_1^2 - \delta_0 \delta_2} t + \delta_0}{\frac{\delta_2}{\delta_1^2 - \delta_0 \delta_2} t^2 - \frac{\delta_1 \delta_2}{\delta_1^2 - \delta_0 \delta_2} t + 1}. \tag{8}$$

The predictions of amplitude growth from the eW-model are also presented in Fig. 5. For small initial  $ma_0$ , a better agreement with the experimental results is achieved. As  $ma_0$  increases, although the eW-model underestimates amplitude growth, it presents a correct development trend.

The amplitudes of bubble and spike in groups I and II are extracted from experiments and predicted by models, as presented in Figs. 6(a) and 6(b). Note that the spike (bubble) radius is smaller (larger) than the balanced position, and thus, the negative (positive) amplitude is defined for the spike (bubble). In convergent geometry, the BP effect always promotes amplitude growths of bubble and spike. This promotion results in a longer linear regime of the spike growth during the time studied. However, the bubble growth quickly saturates

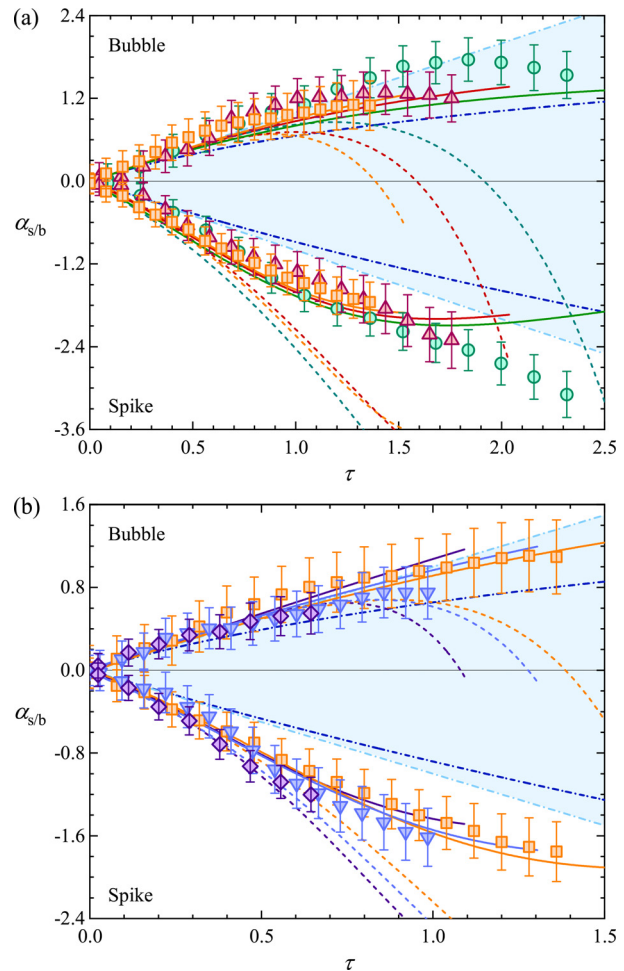


FIG. 6. Amplitude growths of bubble and spike in groups I (a) and II (b). The lines represent the same meaning as those in Fig. 5.



and even reduces. This will be explained later. The ZG model underestimates growths for both spike and bubble due to the promotion by the BP effect. The mW-model well predicts amplitude growths of bubble and spike at early stages but fails to predict them from intermediate stages, probably due to the overestimation of the second-order harmonic. The eW-model has a longer effective time than the mW-model, especially for cases with small initial  $ma_0$ .

To illustrate contributions of the BP effect to bubble and spike growths in cylindrical geometry and explain difference of the BP effect in light-heavy and heavy-light interfaces, a schematic, as shown in Fig. 7, is provided. Here, the BP effects on in-going part and out-going part are considered separately. Assuming that at time  $t$ , the balanced radius of the interface is  $R$ , and the amplitudes of in-going part and out-going part are  $a_i$  and  $a_o$ , respectively. The masses of in-going part ( $M_i$ ) and out-going part ( $M_o$ ) can be expressed as

$$\begin{aligned} M_i &= \rho[\pi R^2 - \pi(R - a_i)^2], \\ M_o &= \rho[\pi(R + a_o)^2 - \pi R^2]. \end{aligned} \tag{9}$$

After time  $\Delta t$ , the balanced radius of the interface, the amplitudes of in-going part and out-going part are  $R' = R + \Delta R$ ,  $a'_i = a_i + \Delta a_i$ , and  $a'_o = a_o + \Delta a_o$ . Taking the out-going part as an example and assuming that the mass is conserved, we have

$$\rho[\pi(R + a_o)^2 - \pi R^2] = (\rho + \Delta\rho)[\pi(R' + a'_o)^2 - \pi R'^2]. \tag{10}$$

After ignoring the high-order terms and note that  $a_o/2R \ll 1$ , we have

$$\Delta a_o = -\frac{Ra_o}{R + a_o} \left( \frac{\Delta\rho}{\rho} + \frac{\Delta R}{R} \right). \tag{11}$$

Following the similar approach, we have

$$\Delta a_i = -\frac{Ra_i}{R - a_i} \left( \frac{\Delta\rho}{\rho} + \frac{\Delta R}{R} \right). \tag{12}$$

Note that the converging velocities of these two parts are different, resulting in perturbation growth. For a heavy-light interface, the in-going parts are spikes, and the out-going parts are bubbles.

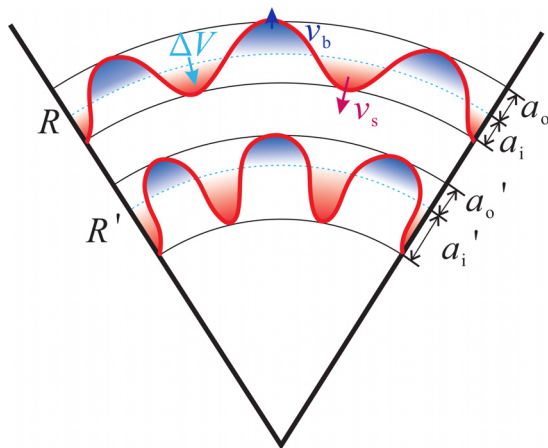


FIG. 7. A schematic diagram of the BP effect on bubble and spike.

Generally, spikes are sharper and longer than bubbles, i.e.,  $\Delta a_s = \Delta a_i > \Delta a_o = \Delta a_b$ . As a result, the spike growth is accelerated more by the BP effect than the bubble growth, which means the BP effect amplifies the discrepancy between spike and bubble growths in convergent RM instability of a heavy-light interface. From the perspective of modal decomposition, the divergence between spike and bubble growths is mainly caused by the second-order harmonic, which the growth rate can be expressed as

$$v_{2rd} \approx \frac{1}{2}(v_s - v_b) \approx \frac{\Delta a_s - \Delta a_b}{2\Delta t}. \tag{13}$$

For a heavy-light interface in convergent geometry, the BP effect promotes generation and development of the second-order harmonic, causing saturation and even reduction of the bubble amplitude. For a light-heavy interface, the BP effect contributes more to bubble growth than spike growth, resulting in different behaviors of bubble and spike growths.

#### IV. CONCLUSIONS

The development of a single-mode SF<sub>6</sub>-air interface subjected to a convergent shock is investigated. To decouple the Bell-Plesset (BP) effect from the Rayleigh-Taylor (RT) effect and the reflected shock, the convergent shock tube is specially designed with an opening end, which allows the convergent shock to leave the test section without focusing. To create a heavy gas environment at the upstream side of the interface, the gas layer scheme is used. An undisturbed interface and a single-mode interface are formed by the soap-film technique, and air between these two interface is replaced by SF<sub>6</sub>. The results show that the RT effect can be ignored, and the effect of reflected waves inside the gas layer is limited.

Five single-mode interfaces with different amplitudes and wavelengths are considered. The schlieren images show that the perturbation amplitude first reduces to zero and then increases in the opposite direction. This process is known as phase inversion. The amplitude reduction is accelerated in the startup process before phase inversion is finished, and the BP effect is found to be negligible in this process. After phase inversion, the amplitude experiences linear and nonlinear growths. In the previous work, the linear growth rate was always not correctly predicted because the BP effect is strong. In this work, shortly after phase inversion, the amplitude is small, and the BP effect is weak. The linear model proposed by Wouchuk and Nishihara<sup>55</sup> roughly predicts the linear growth rate by considering the three-dimensionality correction.

The nonlinear model proposed by Wang *et al.*<sup>27</sup> (mW-model) can only predict the earlier evolution. Based on the Padé approximation, the mW-model is modified to give a better prediction of the amplitude growth. We find that the spike amplitude grows almost linearly, whereas the bubble amplitude gradually saturates and even reduces. For a heavy-light interface in convergent geometry, although both spike and bubble amplitude growths are promoted by the BP effect, the spike amplitude growth is more promoted than the bubble amplitude growth. Moreover, the BP effect enhances generation of the second-order harmonic, which results in saturation and reduction of the bubble amplitude. For a light-heavy interface, the BP effect contributes more to the bubble amplitude growth than the spike amplitude growth. The discrepancy in the BP effect between the light-heavy and heavy-light interfaces is qualitatively demonstrated for the first time.

ACKNOWLEDGMENTS

This work was supported by the National Natural Science Foundation of China (Nos. 12372281, 12022201, 91952205, and 12102425) and Youth Innovation Promotion Association CAS.

AUTHOR DECLARATIONS

Conflict of Interest

The authors have no conflicts to disclose.

Author Contributions

**Jiaxuan Li:** Data curation (equal); Formal analysis (equal); Writing – original draft (equal). **He Wang:** Methodology (equal). **Zhigang Zhai:** Supervision (equal); Writing – review & editing (equal). **Xisheng Luo:** Conceptualization (lead); Funding acquisition (equal).

DATA AVAILABILITY

The data that support the findings of this study are available from the corresponding author upon reasonable request.

APPENDIX: FORMULAS OF THE MW-MODEL

The three orders of the mW-model and the 3rd feedback to 1st can be written as

$$a_{1,1} = a_0 + \dot{a}_0 t C_r, \tag{A1}$$

$$a_{2,2} = a_0 \dot{a}_0 t \left( A \frac{m}{R} - \frac{11}{2R} \right) (C_r - 1) + \dot{a}_0^2 t^2 \left[ \left( \frac{1}{6} A \frac{m}{R} - \frac{11}{4R} \right) C_r^2 - \frac{2}{3} A \frac{m}{R} C_r \right], \tag{A2}$$

$$a_{3,3} = -a_0^3 \frac{1}{8} \left( 3 \frac{m^2}{R^2} - A \frac{1}{R} \frac{m}{R} \right) \left( 1 - 2 \frac{1}{C_r} + \frac{1}{C_r^2} \right) + a_0^2 \dot{a}_0 \frac{1}{8} t \left\{ \left[ (8A^2 - 1) \frac{m^2}{R^2} - 9A \frac{1}{R} \frac{m}{R} + \frac{2}{R^2} \right] C_r - \left[ (16A^2 - 8) \frac{m^2}{R^2} - 8A \frac{1}{R} \frac{m}{R} + \frac{2}{R^2} \right] + \left[ (8A^2 - 7) \frac{m^2}{R^2} + A \frac{1}{R} \frac{m}{R} \right] \frac{1}{C_r} \right\} + a_0 \dot{a}_0^2 \frac{1}{24} t^2 \left\{ \left( 9A^2 \frac{m^2}{R^2} - 26A \frac{1}{R} \frac{m}{R} + \frac{9}{R^2} \right) C_r^2 - 2 \left[ (27A^2 - 3) \frac{m^2}{R^2} - 19A \frac{1}{R} \frac{m}{R} + \frac{3}{R^2} \right] C_r + \left[ 5(3A^2 - 1) \frac{m^2}{R^2} - 2A \frac{1}{R} \frac{m}{R} \right] \right\} + \dot{a}_0^3 t^3 \left\{ \left( \frac{1}{40} A^2 \frac{m^2}{R^2} - \frac{11}{60} A \frac{1}{R} \frac{m}{R} + \frac{1}{8R^2} \right) C_r^3 - \left( \frac{3}{10} A^2 \frac{m^2}{R^2} - \frac{8}{15} A \frac{1}{R} \frac{m}{R} \right) C_r^2 + \left[ \left( \frac{31}{40} A^2 - \frac{1}{8} \right) \frac{m^2}{R^2} + \frac{3}{20} A \frac{1}{R} \frac{m}{R} \right] C_r \right\}, \tag{A3}$$

$$a_{3,1} = a_0^3 \frac{1}{8} \left( 3 \frac{m^2}{R^2} - A \frac{1}{R} \frac{m}{R} \right) \left( 1 - 2 \frac{1}{C_r} + \frac{1}{C_r^2} \right) + a_0^2 \dot{a}_0 \frac{1}{24} t \left\{ - \left[ (8A^2 - 7) \frac{m^2}{R^2} + 19A \frac{1}{R} \frac{m}{R} - 18 \frac{1}{R^2} \right] C_r + 2 \left[ (8A^2 - 10) \frac{m^2}{R^2} + 7A \frac{1}{R} \frac{m}{R} - \frac{3}{R^2} \right] - \left[ (8A^2 - 13) \frac{m^2}{R^2} - 5A \frac{1}{R} \frac{m}{R} + \frac{12}{R^2} \right] \frac{1}{C_r} \right\} + a_0 \dot{a}_0^2 \frac{1}{24} t^2 \left\{ \left( (A^2 + 2) \frac{m^2}{R^2} - 22A \frac{1}{R} \frac{m}{R} + 27 \frac{1}{R^2} \right) C_r^2 + 2 \left[ (5A^2 - 5) \frac{m^2}{R^2} + 13A \frac{1}{R} \frac{m}{R} - 3 \frac{1}{R^2} \right] C_r - \left[ (11A^2 - 5) \frac{m^2}{R^2} - 2A \frac{1}{R} \frac{m}{R} \right] \right\} + \dot{a}_0^3 t^3 \left\{ \left( \frac{1}{120} A^2 \frac{m^2}{R^2} - \frac{11}{60} A \frac{1}{R} \frac{m}{R} + \frac{3}{8R^2} \right) C_r^3 - \left[ \left( \frac{1}{60} A^2 + \frac{1}{12R^2} \right) - \frac{11}{30} A \frac{1}{R} \frac{m}{R} \right] C_r^2 - \left[ \left( \frac{19}{120} A^2 - \frac{1}{24} \right) \frac{m^2}{R^2} + \frac{1}{60} A \frac{1}{R} \frac{m}{R} \right] C_r \right\}, \tag{A4}$$

where  $C_r = R_0/R(t)$  is the convergent ratio and  $\dot{a}_0$  is the initial growth rate.

The amplitude of bubbles and spikes can be written as

$$a_{s/b} = \mp (a_{1,1} \pm a_{2,2} + a_{3,3} + a_{3,1}). \tag{A5}$$

REFERENCES

- <sup>1</sup>R. D. Richtmyer, “Taylor instability in shock acceleration of compressible fluids,” *Commun. Pure Appl. Math.* **13**, 297–319 (1960).
- <sup>2</sup>E. E. Meshkov, “Instability of the interface of two gases accelerated by a shock wave,” *Fluid Dyn.* **4**, 101–104 (1969).
- <sup>3</sup>L. Rayleigh, “Investigation of the character of the equilibrium of an incompressible heavy fluid of variable density,” *Proc. London Math. Soc.* **s1-14**, 170–177 (1882).
- <sup>4</sup>G. Taylor, “The instability of liquid surfaces when accelerated in a direction perpendicular to their planes. I,” *Proc. R. Soc. London, Ser. A* **201**, 192–196 (1950).
- <sup>5</sup>J. Lindl, O. Landen, J. Edwards, and E. Moses, and NIC Team. “Review of the national ignition campaign 2009–2012,” *Phys. Plasmas* **21**, 020501 (2014).
- <sup>6</sup>J. Shimoda, T. Inoue, Y. Ohira, R. Yamazaki, A. Bamba, and J. Vink, “On cosmic-ray production efficiency at supernova remnant shocks propagating into realistic diffuse interstellar medium,” *Astrophys. J.* **803**, 98 (2015).
- <sup>7</sup>R. V. Morgan, R. Aure, J. D. Stockero, J. A. Greenough, W. Cabot, O. A. Likhachev, and J. W. Jacobs, “On the late-time growth of the two-dimensional Richtmyer-Meshkov instability in shock tube experiments,” *J. Fluid Mech.* **712**, 354–383 (2012).
- <sup>8</sup>B. J. Balakumar, G. C. Orlicz, J. R. Ristorcelli, S. Balasubramanian, K. P. Prestridge, and C. D. Tomkins, “Turbulent mixing in a Richtmyer-Meshkov fluid layer after reshock: Velocity and density statistics,” *J. Fluid Mech.* **696**, 67–93 (2012).
- <sup>9</sup>M. Vandenboomgaerde, D. Souffland, C. Mariani, L. Biamino, G. Jourdan, and L. Houas, “An experimental and numerical investigation of the dependency on the initial conditions of the Richtmyer-Meshkov instability,” *Phys. Fluids* **26**, 024109 (2014).
- <sup>10</sup>K. A. Meyer and P. J. Blewett, “Numerical investigation of the stability of a shock-accelerated interface between two fluids,” *Phys. Fluids* **15**, 753–759 (1972).

- <sup>11</sup>G. Jourdan and L. Houas, "High-amplitude single-mode perturbation evolution at the Richtmyer-Meshkov instability," *Phys. Rev. Lett.* **95**, 204502 (2005).
- <sup>12</sup>C. Mariani, M. Vandenboomgaerde, G. Jourdan, D. Souffland, and L. Houas, "Investigation of the Richtmyer-Meshkov instability with stereolithographed interfaces," *Phys. Rev. Lett.* **100**, 254503 (2008).
- <sup>13</sup>X. Guo, T. Si, Z. Zhai, and X. Luo, "Large-amplitude effects on interface perturbation growth in Richtmyer-Meshkov flows with reshock," *Phys. Fluids* **34**, 082118 (2022).
- <sup>14</sup>G. I. Bell, "Taylor instability on cylinders and spheres in the small amplitude approximation," Report No. LA-1321, LANL 1321, 91873-918739 (1951).
- <sup>15</sup>M. S. Plesset, "On the stability of fluid flows with spherical symmetry," *J. Appl. Phys.* **25**, 96-98 (1954).
- <sup>16</sup>M. Lombardini, D. I. Pullin, and D. I. Meiron, "Turbulent mixing driven by spherical implosions. Part 1. Flow description and mixing-layer growth," *J. Fluid Mech.* **748**, 85-112 (2014).
- <sup>17</sup>J. Ding, T. Si, J. Yang, X. Lu, Z. Zhai, and X. Luo, "Measurement of a Richtmyer-Meshkov instability at an air-SF<sub>6</sub> interface in a semiannular shock tube," *Phys. Rev. Lett.* **119**, 014501 (2017).
- <sup>18</sup>C. Samulski, B. Srinivasan, M. J.-E. Manuel, R. L. Masti, J. P. Sauppe, and J. Kline, "Deceleration-stage Rayleigh-Taylor growth in a background magnetic field studied in cylindrical and Cartesian geometries," *Matter Radiat. Extremes* **7**, 026902 (2022).
- <sup>19</sup>K. O. Mikaelian, "Rayleigh-Taylor and Richtmyer-Meshkov instabilities and mixing in stratified spherical shells," *Phys. Rev. A* **42**, 3400-3420 (1990).
- <sup>20</sup>K. O. Mikaelian, "Stability and mix in spherical geometry," *Phys. Rev. Lett.* **65**, 992-995 (1990).
- <sup>21</sup>K. O. Mikaelian, "Rayleigh-Taylor and Richtmyer-Meshkov instabilities and mixing in stratified cylindrical shells," *Phys. Fluids* **17**, 094105 (2005).
- <sup>22</sup>M. Lombardini and D. I. Pullin, "Small-amplitude perturbations in the three-dimensional cylindrical Richtmyer-Meshkov instability," *Phys. Fluids* **21**, 114103 (2009).
- <sup>23</sup>C. Matsuoka and K. Nishihara, "Analytical and numerical study on a vortex sheet in incompressible Richtmyer-Meshkov instability in cylindrical geometry," *Phys. Rev. E* **74**, 066303 (2006).
- <sup>24</sup>W. H. Liu, X. T. He, and C. P. Yu, "Cylindrical effects on Richtmyer-Meshkov instability for arbitrary Atwood numbers in weakly nonlinear regime," *Phys. Plasmas* **19**, 072108 (2012).
- <sup>25</sup>W. H. Liu, C. P. Yu, W. H. Ye, L. F. Wang, and X. T. He, "Nonlinear theory of classical cylindrical Richtmyer-Meshkov instability for arbitrary Atwood numbers," *Phys. Plasmas* **21**, 062119 (2014).
- <sup>26</sup>L. Wang, J. Wu, W. Ye, W. Zhang, and X. He, "Weakly nonlinear incompressible Rayleigh-Taylor instability growth at cylindrically convergent interfaces," *Phys. Plasmas* **20**, 042708 (2013).
- <sup>27</sup>L. F. Wang, J. F. Wu, H. Y. Guo, W. H. Ye, J. Liu, W. Y. Zhang, and X. T. He, "Weakly nonlinear Bell-Plesset effects for a uniformly converging cylinder," *Phys. Plasmas* **22**, 082702 (2015).
- <sup>28</sup>J. Ge, H. Li, X. Zhang, and B. Tian, "Evaluating the stretching/compression effect of Richtmyer-Meshkov instability in convergent geometries," *J. Fluid Mech.* **946**, A18 (2022).
- <sup>29</sup>V. N. Goncharov, "Analytical model of nonlinear, single-mode, classical Rayleigh-Taylor instability at arbitrary Atwood numbers," *Phys. Rev. Lett.* **88**, 134502 (2002).
- <sup>30</sup>Z. Zhao, P. Wang, N. Liu, and X. Lu, "Analytical model of nonlinear evolution of single-mode Rayleigh-Taylor instability in cylindrical geometry," *J. Fluid Mech.* **900**, A24 (2020).
- <sup>31</sup>W. Mostert, D. I. Pullin, V. Wheatley, and R. Samtaney, "Magnetohydrodynamic implosion symmetry and suppression of Richtmyer-Meshkov instability in an octahedrally symmetric field," *Phys. Rev. Fluids* **2**, 013701 (2017).
- <sup>32</sup>A. Bakhsh and R. Samtaney, "Incompressible models of magnetohydrodynamic Richtmyer-Meshkov instability in cylindrical geometry," *Phys. Rev. Fluids* **4**, 063906 (2019).
- <sup>33</sup>A. Bakhsh, "Linear analysis of magnetohydrodynamic Richtmyer-Meshkov instability in cylindrical geometry for double interfaces in the presence of an azimuthal magnetic field," *Phys. Rev. Fluids* **34**, 114120 (2022).
- <sup>34</sup>Y. Li, R. Samtaney, D. Bond, and V. Wheatley, "Richtmyer-Meshkov instability of an imploding flow with a two-fluid plasma model," *Phys. Rev. Fluids* **5**, 113701 (2020).
- <sup>35</sup>J. Wu, H. Liu, and Z. Xiao, "Refined modelling of the single-mode cylindrical Richtmyer-Meshkov instability," *J. Fluid Mech.* **908**, A9 (2021).
- <sup>36</sup>J. Li, J. Ding, X. Luo, and Z. Zou, "Instability of a heavy gas layer induced by a cylindrical convergent shock," *Phys. Fluids* **34**, 042123 (2022).
- <sup>37</sup>S. H. R. Hosseini and K. Takayama, "Experimental study of Richtmyer-Meshkov instability induced by cylindrical shock waves," *Phys. Fluids* **17**, 084101 (2005).
- <sup>38</sup>L. Biamino, G. Jourdan, C. Mariani, L. Houas, M. Vandenboomgaerde, and D. Souffland, "On the possibility of studying the converging Richtmyer-Meshkov instability in a conventional shock tube," *Exp. Fluids* **56**, 1-5 (2015).
- <sup>39</sup>M. Vandenboomgaerde, P. Rouzier, D. Souffland, L. Biamino, G. Jourdan, L. Houas, and C. Mariani, "Nonlinear growth of the converging Richtmyer-Meshkov instability in a conventional shock tube," *Phys. Rev. Fluids* **3**, 014001 (2018).
- <sup>40</sup>X. Luo, F. Zhang, J. Ding, T. Si, J. Yang, Z. Zhai, and C. Wen, "Long-term effect of Rayleigh-Taylor stabilization on converging Richtmyer-Meshkov instability," *J. Fluid Mech.* **849**, 231-244 (2018).
- <sup>41</sup>Z. Zhai, F. Zhang, Z. Zhou, J. Ding, and C. Wen, "Numerical study on Rayleigh-Taylor effect on cylindrically converging Richtmyer-Meshkov instability," *Sci. China-Phys. Mech. Astron.* **62**, 124712 (2019).
- <sup>42</sup>X. Luo, M. Li, J. Ding, Z. Zhai, and T. Si, "Nonlinear behaviour of convergent Richtmyer-Meshkov instability," *J. Fluid Mech.* **877**, 130-141 (2019).
- <sup>43</sup>Y. Liang and X. Luo, "On shock-induced heavy-fluid-layer evolution," *J. Fluid Mech.* **920**, A13 (2021).
- <sup>44</sup>M. Li, J. Ding, Z. Zhai, T. Si, N. Liu, S. Huang, and X. Luo, "On divergent Richtmyer-Meshkov instability of a light/heavy interface," *J. Fluid Mech.* **901**, A38 (2020).
- <sup>45</sup>X. Guo, J. Ding, X. Luo, and Z. Zhai, "Evolution of a shocked multimode interface with sharp corners," *Phys. Rev. Fluids* **3**, 114004 (2018).
- <sup>46</sup>X. Guo, Z. Zhai, T. Si, and X. Luo, "Bubble merger in initial Richtmyer-Meshkov instability on inverse-chevron interface," *Phys. Rev. Fluids* **4**, 092001 (R) (2019).
- <sup>47</sup>H. Wang, H. Wang, Z. Zhai, and X. Luo, "Effects of obstacles on shock-induced perturbation growth," *Phys. Fluids* **34**, 086112 (2022).
- <sup>48</sup>J. Xu, H. Wang, Z. Zhai, and X. Luo, "Convergent Richtmyer-Meshkov instability on two-dimensional dual-mode interfaces," *J. Fluid Mech.* **965**, A8 (2023).
- <sup>49</sup>Y. Liang, L. Liu, Z. Zhai, T. Si, and C. Wen, "Evolution of shock-accelerated heavy gas layer," *J. Fluid Mech.* **886**, A7 (2020).
- <sup>50</sup>X. Luo, B. Guan, T. Si, Z. Zhai, and X. Wang, "Richtmyer-Meshkov instability of a three-dimensional SF<sub>6</sub>-air interface with a minimum-surface feature," *Phys. Rev. E* **93**, 013101 (2016).
- <sup>51</sup>M. Lombardini and D. I. Pullin, "Startup process in the Richtmyer-Meshkov instability," *Phys. Fluids* **21**, 044104 (2009).
- <sup>52</sup>Y. Yang, Q. Zhang, and D. H. Sharp, "Small amplitude theory of Richtmyer-Meshkov instability," *Phys. Fluids* **6**, 1856-1873 (1994).
- <sup>53</sup>J. Li, J. Ding, T. Si, and X. Luo, "Convergent Richtmyer-Meshkov instability of light gas layer with perturbed outer surface," *J. Fluid Mech.* **884**, R2 (2020).
- <sup>54</sup>Z. Zhai, P. Dong, T. Si, and X. Luo, "The Richtmyer-Meshkov instability of a 'V' shaped air/helium interface subjected to a weak shock," *Phys. Fluids* **28**, 082104 (2016).
- <sup>55</sup>J. Wouchuk and K. Nishihara, "Asymptotic growth in the linear Richtmyer-Meshkov instability," *Phys. Plasmas* **4**, 1028-1038 (1997).
- <sup>56</sup>Q. Zhang and W. Guo, "Universality of finger growth in two-dimensional Rayleigh-Taylor and Richtmyer-Meshkov instabilities with all density ratios," *J. Fluid Mech.* **786**, 47-61 (2016).